Electron Hopping through Double-Exchange Coupling in a Mixed-Valence Diiminobenzoquinone-Bridged Fe₂ Complex

Alexandra I. Gaudette,[†] Ie-Rang Jeon,[†] John S. Anderson,[†,§] Fernande Grandjean,[‡] Gary J. Long,[‡] and T. David Harris*,[†]

[†]Department of Chemistry, Northwestern University, Evanston, Illinois 60208-3113, United States

[‡]Department of Chemistry, Missouri University of Science and Technology, University of Missouri, Rolla, Missouri 65409-0010, United States

Ⓢ *Supporting Information*

ABSTRACT: The ability of a benzoquinonoid bridging ligand to mediate double-exchange coupling in a mixed-valence Fe₂ complex is demonstrated. Metalation of the bridging ligand 2,5-di(2,6-dimethylanilino)-3,6-dibromo-1,4-benzoquinone (LH_2) with Fe^{II} in the presence of the capping ligand tris((6-methyl-2-pyridyl)methyl)amine (Me_3TPyA) affords the dinuclear complex $[(Me_3TPyA)_2Fe^{II}_2(L)]^{2+}$. The dc magnetic measurements, in conjunction with X-ray diffraction and Mössbauer spectroscopy, reveal the presence of weak ferromagnetic superexchange coupling between Fe^{II} centers through the diamagnetic bridging ligand to give an $S = 4$ ground state. The ac magnetic susceptibility measurements, collected in a small dc field, show this complex to behave as a

weak superexchange   *strong double-exchange*

single-molecule magnet with a relaxation barrier of $U_{eff} = 14(1)$ cm^{-1}. The slow magnetic relaxation in the Fe^{II}_2 complex can be switched off through one-electron oxidation to the mixed-valence congener $[(Me_3TPyA)_2Fe_2(L)]^{3+}$, where X-ray diffraction and Mössbauer spectroscopy indicate a metal-centered oxidation. The dc magnetic measurements show an $S = \frac{9}{2}$ ground state for the mixed-valence complex, stemming from strong ferromagnetic exchange coupling that is best described considering electron hopping through a double-exchange coupling mechanism, with a double-exchange parameter of $B = 69(4)$ cm^{-1}. In accordance with double-exchange, an intense feature is observed in the near-infrared region and is assigned as an intervalence charge-transfer band. The rate of intervalence electron hopping is comparable to that of the Mössbauer time scale, such that variable-temperature Mössbauer spectra reveal a thermally activated transition from a valence-trapped to detrapped state and provide an activation energy for electron hopping of $63(8)$ cm^{-1}. These results demonstrate the ability of quinonoid ligands to mediate electron hopping between high-spin metal centers, by providing the first example of an Fe complex that exhibits double-exchange through an organic bridging ligand and the largest metal–metal separation yet observed in any metal complex with double-exchange coupling.
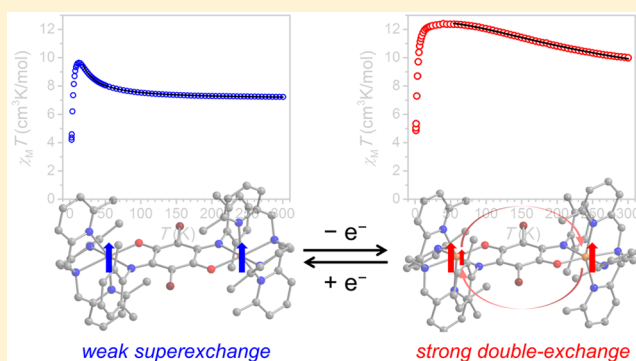
INTRODUCTION

Over the past two decades, a number of molecules have been shown to exhibit slow magnetic relaxation upon removal of an applied external magnetic field, thereby mimicking the behavior previously only associated with bulk magnets.[1] These discrete molecular complexes, which have come to be known as single-molecule magnets, may find use in applications such as high-density spin-based information storage and processing.[2] To date, single-molecule magnets have taken the form of multi- and mononuclear complexes containing transition metals,[3,4] lanthanides,[5,6] and actinides,[7,8] and have been shown to exhibit spin relaxation barriers of up to 652 cm^{-1} [6d] and magnetic blocking temperatures of up to 14 K.[5c] In an effort to further increase the relaxation barriers and blocking temperatures in single-molecule magnets, researchers have focused on maximizing the spin ground state (S) and the axial zero-field splitting parameter (D) of these molecules, as the magnitude of the relaxation barrier is given as $U = S^2|D|$.

In addition to the critical parameters S and D, the strength of magnetic interaction between spin centers in a molecule should also be maximized, as this value is directly correlated to the energetic isolation of the ground state from excited states.[9] Moreover, strong coupling is also necessary for the high-temperature function of higher-dimensional magnets, as the relaxation barrier in single-chain magnets[10] and the ordering temperature in bulk magnets[11] are both proportional to the strength of magnetic exchange interactions between spin carriers. One strategy toward this end is the installation of electron hopping between metal centers in a mixed-valence complex, which can give rise to very strong ferromagnetic

Table 1. Crystallographic Data for 1 and 2

	1	2
formula	$C_{128}H_{90}B_2Br_2F_{48}Fe_2N_{10}O_2$	$C_{161}H_{104}B_3Br_2Cl_2F_{72}Fe_2N_{10}O_2$
fw (g/mol)	3005.23	3953.39
space group	$P\bar{1}$	$P\bar{1}$
wavelength (Å)	1.54178	1.54178
temp (K)	100	100
a (Å)	12.2741(5)	16.461(6)
b (Å)	20.2397(8)	23.978(9)
c (Å)	26.2330(10)	46.22(2)
α (deg)	88.986(2)	74.978(12)
β (deg)	88.420(2)	89.070(15)
γ (deg)	78.267(2)	71.113(9)
V (Å^3)	6377.8(4)	16625(11)
Z	2	4
d_{calcd} (g cm^{-3})	1.565	1.579
R_{int}	0.0296	0.0986
$R_1{}^a$ $(I > 2\sigma(I))$	0.0901	0.1286
$wR_2{}^b$ (all)	0.2594	0.3523
GoF	1.024	0.972

$^a R_1 = \Sigma ||F_0| - |F_C|| / \Sigma |F_0|$. $^b wR_2 = [\Sigma w(F_0{}^2 - F_C{}^2)^2 / \Sigma w(F_0{}^2)^2]^{1/2}$.

interactions between high-spin metal centers via a double-exchange mechanism.[12] Indeed, several classes of mixed-valence Fe_2 complexes with $S = {}^9/_2$ ground states mediated by double-exchange interactions have been isolated and studied, with Fe_2 cores supported by hydroxo,[13] phenoxo,[14] alkoxo,[15] and carboxylato[16] bridging ligands. Similarly, a number of iron–sulfur clusters in biology have been shown to exhibit double-exchange that is mediated through sulfido bridges in Fe_2 units.[17]

Notably, all of the above complexes and metalloproteins that exhibit double-exchange coupling feature direct Fe···Fe orbital interactions and/or single-atom inorganic bridging ligands, which serve to mediate the double-exchange interactions. As an alternative, the employment of organic bridging ligands would provide new synthetic opportunities for high-nuclearity molecules and high-dimensional solids with strong magnetic coupling and itinerant electrons, owing to the ability of these ligands to accommodate extensive chemical modification and to enable rational chemical design and synthesis. Despite this potential, to date no organic ligand-bridged Fe_2 complex has been shown to exhibit a high-spin ground state through double-exchange. In fact, an imidazolate-bridged $[V_2]^V$ complex provides the only example of organic ligand-based double-exchange in any metal complex, which was shown to exhibit a well-isolated $S = {}^5/_2$ ground state through a double-exchange interaction.[18]

When considering potential organic bridging ligands to mediate double-exchange in mixed-valence molecules, quinonoid-type ligands offer two key potential attributes. First, a number of dinuclear benzoquinonoid-bridged mixed-valence complexes have been shown to support electron delocalization, albeit only in low-spin molecules.[19−22] In addition, the extensive chemical modularity of these ligands offers the possibility to precisely tune the thermodynamics and kinetics of electron transfer. Herein, we report the synthesis and characterization of two redox isomers of a diiminobenzoquinone-bridged Fe_2 complex, $[(Me_3TPyA)_2Fe_2(L)]^{n+}$ (n = 2, 3). The latter isomer, which features a mixed-valence $[Fe_2]^V$ core, exhibits an $S = {}^9/_2$ ground state, with magnetic susceptibility and spectroscopic measurements indicating the presence of

electron hopping between Fe centers. In addition, variable-temperature Mössbauer spectra reveal the transition from a valence-trapped to detrapped state with increasing temperature. To the best of our knowledge, this mixed-valence molecule is the first example of an iron complex with double-exchange through an organic bridging ligand, and it features the largest metal–metal separation yet observed in any metal complex involving a double-exchange mechanism.

■ **EXPERIMENTAL SECTION**

General Considerations. Unless otherwise noted, the manipulations described below were performed under a dinitrogen atmosphere in a Vacuum Atmospheres Nexus II glovebox. Glassware was oven-dried at 150 °C for at least 4 h and allowed to cool in an evacuated antechamber prior to use in the glovebox. Tetrahydrofuran, dichloromethane, and hexanes were dried using a commercial solvent purification system from Pure Process Technology and stored over 3 or 4 Å molecular sieves prior to use. Deuterated solvents were purchased from Cambridge Isotope Laboratories or Sigma-Aldrich, deoxygenated by three successive freeze–pump–thaw cycles, and stored over 3 or 4 Å molecular sieves prior to use. Hexanes and tetrahydrofuran were typically tested with a standard purple solution of sodium benzophenone ketyl in THF in order to confirm effective oxygen and moisture removal. The compounds $[Fe(MeCN)_6]$-$(BAr^F_4)_2$,[23] $[N(4\text{-}BrC_6H_4)_3](BAr^F_4)$,[24] tris((6-methyl-2-pyridyl)-methyl)amine (Me_3TPyA),[25] and lithium bis(trimethylsilyl)amide $(Li[N(SiMe_3)_2])$[26] were prepared according to literature procedures. All other reagents were purchased from commercial vendors and used without further purification.

2,5-Di(2,6-dimethylanilino)-3,6-dibromo-1,4-benzoquinone (LH$_2$). In air, 2,6-dimethylaniline (2.28 g, 18.8 mmol) was added dropwise to a slurry of 2,3,5,6-tetrabromo-1,4-benzoquinone (2.00 g, 4.72 mmol) and sodium acetate (1.54 g, 18.8 mmol) in 80 mL EtOH at 60 °C. The reaction mixture was then heated at reflux for 48 h, resulting in the precipitation of a red solid. This solid was collected via vacuum filtration, washed with H_2O (10 mL), EtOH (10 mL), and hexanes (10 mL), and then was dried under reduced pressure for 12 h to yield LH$_2$ as a red solid (0.655 g, 28%). ^{1}H NMR (DMSO-d_6): 9.61 (s, 2H) 7.14 (t, 2H) 7.05 (d, 4H) 2.10 (s, 12H).

$[(Me_3TPyA)_2Fe_2(L)](BAr^F_4)_2$ (1). Me_3TPyA (0.112 g, 0.337 mmol) was dissolved in THF (2 mL), and the resulting solution was added dropwise with stirring to a solution of $[Fe(MeCN)_6](BAr^F_4)_2$ (0.683 g, 0.337 mmol) in THF (3 mL). The resulting yellow solution was

stirred for 5 min at ambient temperature, and to it was added a slurry of LH_2 (0.085 g, 0.19 mmol) in THF (2 mL). To this mixture, a solution of $Li[N(SiMe_3)_2]$ (0.056 g, 0.34 mmol) in THF (2 mL) was added dropwise with stirring, resulting in a dark green solution. After stirring at ambient temperature for 15 min, the solution was filtered through diatomaceous earth. Layering of the filtrate with hexanes produced a mixture of dark brown-green and colorless microcrystalline solid. This solid mixture was washed with cold EtOH (1 mL), and the residual dark green microcrystalline solid was dissolved in THF (4 mL). Layering of hexanes (16 mL) onto the resulting solution gave **1** (0.208 g, 21%) as dark green plate-shaped crystals suitable for single-crystal X-ray diffraction. Anal. Calcd for $C_{128}H_{90}B_2Br_2F_{48}Fe_2N_{10}O_2$: C, 51.1; H, 3.05; N, 4.65%. Found: C, 51.25; H, 3.06; N, 4.56%.

[(Me₃TPyA)₂Fe₂(L)](BArF₄)₃·CH₂Cl₂ **(2)**. A solution of [N(4-BrC₆H₄)₃](BArF₄) (50 mg, 0.035 mmol) in CH_2Cl_2 (4 mL) was cooled to −78 °C and then was added dropwise with stirring to a solution of **1** (100 mg, 0.033 mmol) in CH_2Cl_2 (4 mL) at −78 °C to give a dark red-purple solution. This solution was filtered through diatomaceous earth, and then layered with hexanes (10 mL) at −78 °C to give dark red-purple plate-shaped crystals suitable for single-crystal X-ray diffraction. These crystals were collected via vacuum filtration and washed with cold 1:1 CH_2Cl_2/hexanes (20 mL) to afford 86 mg (63%) of **2**. Anal. Calcd for $C_{161}H_{104}B_3Br_2Cl_2F_{72}Fe_2N_{10}O_2$: C, 48.9; H, 2.65; N, 3.54%. Found: C, 49.74; H, 2.92; N, 3.46%

X-ray Structure Determination. Single crystals of **1** and **2** suitable for X-ray analysis were coated with deoxygenated Paratone-N oil and mounted on a MicroMounts rod. Crystallographic data were collected at 100 K using a Bruker Kappa Apex II diffractometer equipped with an APEX-II detector, a Cu Kα microfocus source, and MX Optics. Raw data were integrated and corrected for Lorentz and polarization effects with SAINT v8.27B.[27] Absorption corrections were applied using SADABS for **1** and **2**. Space group assignments were determined by examination of systematic absences, E-statistics, and successive refinement of the structures. Structures were solved with SHELXT[28] and further refined with SHELXL[29] operated with the Olex2 interface.[30] The SADI restraint was applied to all atoms of the [BArF₄]⁻ counterions in **1** due to disorder. Positional disorder in several trifluoromethyl groups was modeled with partial occupancies. The enhanced rigid-bond restraint (SHELX keyword RIGU) was applied globally in **2**.[31] Positional disorder in the trifluoromethyl groups on the [BArF₄]⁻ counterions were modeled with partial occupancies. All hydrogen atoms were placed at calculated positions using suitable riding models and refined using isotropic displacement parameters derived from their parent atoms. Thermal parameters were refined anisotropically for all non-hydrogen atoms. Crystallographic data and the details of data collection are listed in Table 1. Crystals of both **1** and **2** diffracted weakly, resulting in high R_1 values and low precision on bond lengths. The data collection for **2** was further complicated by decomposition of the crystal during the data collection. Attempts to obtain better data sets for **1** and **2** have thus far been unsuccessful.

Magnetic Measurements. Magnetic measurements of **1** and **2** were performed on polycrystalline samples sealed in polyethylene bags under a dinitrogen atmosphere. All data were collected using a Quantum Design MPMS-XL SQUID magnetometer from 1.8 to 300 K at applied dc fields ranging from 0 to +7 T. Ac magnetic susceptibility data were collected under a dc field of 750 Oe and an ac field of 4 Oe, oscillating at frequencies in the range 10−1500 Hz. Ac susceptibility data were used to construct Cole−Cole plots, which were then fit using a generalized Debye model[32] in the temperature range 1.8−2.4 K to estimate relaxation times. Dc susceptibility data were corrected for diamagnetic contributions from the sample holder and for the core diamagnetism of each sample estimated using Pascal's constants.[33] M vs H curves, constructed from data collected from 0 to 4 T at 100 K, confirmed the absence of ferromagnetic impurities.

Other Physical Measurements. Elemental analyses of **1** and **2** were performed by the Midwest Microlab (Indianapolis, IN). Infrared spectra were recorded on a Bruker Alpha FTIR spectrometer equipped with an attenuated total reflectance accessory. UV−vis−NIR spectra were obtained using a Varian Cary 5000 spectrophotometer. Cyclic

voltammetry measurements were carried out in a standard one-compartment cell under dinitrogen, equipped with platinum wires as counter/working electrodes and a silver wire as reference electrode using a CHI 760c potentiostat. Analyte solutions were prepared with 0.1 M solutions of $(Bu_4N)PF_6$ in CH_2Cl_2. Ferrocene was used as an internal standard, and all potentials were referenced to the $[Cp_2Fe]^{0/1+}$ couple. Zero-field iron-57 Mössbauer spectra were obtained between 5 and 260 K with a constant acceleration spectrometer and a cobalt-57 rhodium source. Prior to the measurements, the spectrometer was calibrated at 295 K with α-iron foil. Samples were prepared in a dinitrogen-filled glovebox and frozen in liquid nitrogen prior to handling in air.

■ RESULTS AND DISCUSSION

Syntheses, Structures, and Cyclic Voltammetry. Reaction of $[Fe(MeCN)_6](BArF_4)_2$ with Me_3TPyA in MeCN, followed by treatment with a mixture of LH_2 and $Li[N-(SiMe_3)_2]$, resulted in a dark green solution. Subsequent liquid diffusion of hexanes into this solution gave dark green plate-shaped crystals of $[(Me_3TPyA)_2Fe_2(L)](BArF_4)_2$ (**1**) in 21% yield. The asymmetric unit of the crystal structure of **1** features two halves of the $[(Me_3TPyA)_2Fe_2(L)]^{2+}$ cation, with the remainder of each cationic complex related through a crystallographic center of inversion (see Figure 1, upper), affording a structure with two crystallographically distinct dinuclear cationic complexes. Each Fe^{II} center resides in a distorted octahedral coordination environment, with nitrogen and oxygen donor atoms of L^{2-} occupying two cis oriented sites and the four nitrogen atoms of Me_3TPyA occupying the
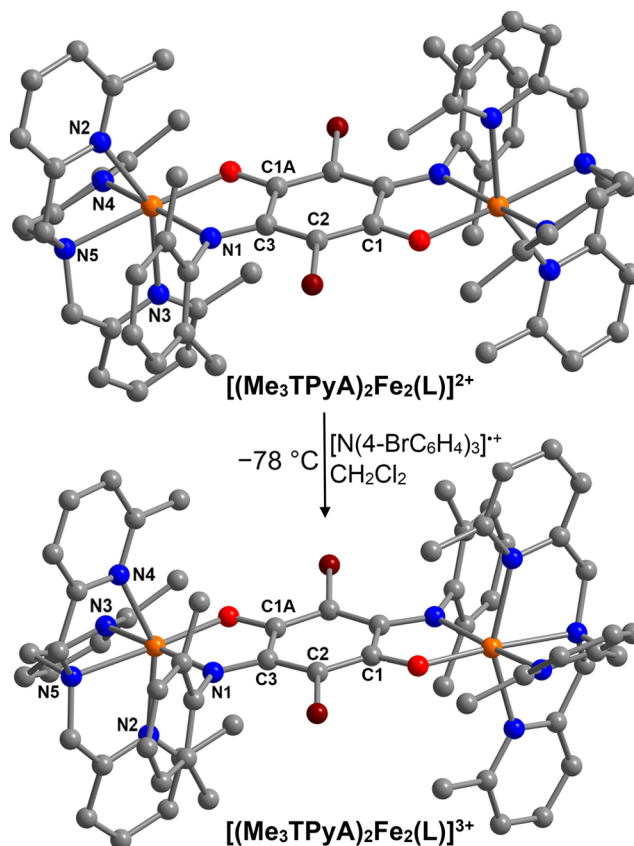
Figure 1. Oxidation of $[(Me_3TPyA)_2Fe_2(L)]^{2+}$ (upper) to give $[(Me_3TPyA)_2Fe_2(L)]^{3+}$ (lower). Orange, maroon, red, blue, and gray spheres represent Fe, Br, O, N, and C atoms, respectively; H atoms are omitted for clarity.

Table 2. Selected Mean Interatomic Distances (Å) in 1 and 2 at 100 K

	1	2		1	2
Fe–N2	2.319(7)	2.23(2)	C1–C2	1.37(1)	1.38(3)
Fe–N3	2.303(7)	2.21(2)	C2–C3	1.43(2)	1.46(3)
Fe–N4	2.233(8)	2.25(2)	C3–C1A	1.51(1)	1.49(3)
Fe–N5	2.203(6)	2.15(2)	C–C$_{avg}$	1.43(1)	1.44(3)
Fe–N$_{TPyA,avg}$	2.264(7)	2.21(2)	N1–C2	1.30(1)	1.32(2)
Fe–N1	2.244(7)	2.13(2)	O1–C3	1.289(8)	1.28(2)
Fe–O1	1.972(6)	1.94(1)	Fe···Fe$_{intra}$	8.126(2)	8.029(4)

remaining sites. Within L^{2-}, the average C–O distance of 1.289(8) Å falls nearly midway between that expected for a single and a double bond (see Table 2). In addition, the average C–N distance of 1.30(1) Å is in close agreement with a double bond. Accordingly, L^{2-} is therefore best described by a resonance form comprising two hydroxo and two imino donors, as has been observed previously in related complexes of iron, cobalt, and ruthenium.[34−38] The average Fe–O and Fe–N distances of 1.972(6) and 2.244(7) Å, respectively, are indicative of high-spin $S = 2$ Fe^{II} centers and support the above description of L^{2-}. Finally, the structure of **1** features a mean intramolecular Fe···Fe distance of 8.126(2) Å and a closest intermolecular Fe···Fe distance of 9.618(2) Å.

The cyclic voltammogram of a CH_2Cl_2 solution of **1**, shown in Figure 2, exhibits three reversible redox processes, centered at $E_{1/2}$ = +0.704, + 0.364, and −1.45 V vs $[Cp_2Fe]^{0/1+}$, with an open-circuit voltage of −0.83 V. On the basis of precedent in other benzoquinonoid-bridged Fe complexes, we assign the wave at negative potential to a ligand-based $L^{2-/3-\bullet}$ process and the two waves at positive potential to metal-based $Fe^{II/III}$ processes.[21h] The potential separation of $\Delta E_{1/2}$ = 0.340 V between the metal-based waves corresponds to a comproportionation constant of K_c = 5.52 × 10^5 for the reaction $[(Me_3TPyA)_2Fe_2(L)]^{2+}$ + $[(Me_3TPyA)_2Fe_2(L)]^{4+}$ → $2[(Me_3TPyA)_2Fe_2(L)]^{3+}$, which suggests that the mixed-valence species $[(Me_3TPyA)_2Fe_2(L)]^{3+}$ can be chemically isolated. Toward this end, a solution of **1** in CH_2Cl_2 was treated at −78 °C with one equivalent of the iminium radical cation-containing oxidant $[N(4-BrC_6H_4)_3](BAr^F_4)$[24,39] to give a dark red-purple solution. Monitoring of this reaction in CD_2Cl_2 by ^1H NMR revealed the complete consumption of **1** with concomitant formation of a new paramagnetic species (see
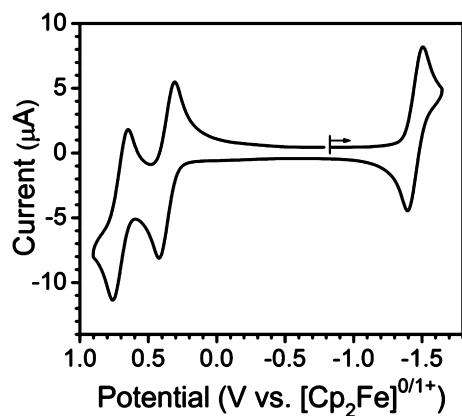

Figure 2. Cyclic voltammogram obtained for a CH_2Cl_2 solution of **1** using a glassy carbon working electrode, 50 mV/s scan rate, and 0.1 M $(Bu_4N)PF_6$ supporting electrolyte.

Figure S1 in the Supporting Information). Layering of cold hexanes onto this solution afforded dark red-purple plate-shaped crystals of $[(Me_3TPyA)_2Fe_2(L)](BAr^F_4)_3\cdot CH_2Cl_2$ (**2**) in 63% yield upon storage at −78 °C.

The crystal structure of **2** at 100 K exhibits an asymmetric unit that contains one full molecule of $[(Me_3TPyA)_2Fe_2(L)]^{3+}$, where the two iron centers are crystallographically inequivalent, along with two halves of different molecules of $[(Me_3TPyA)_2Fe_2(L)]^{3+}$, with the remaining half of each molecule related through a crystallographic inversion center (see Figure 1, lower). Despite the presence of four crystallographically unique Fe centers in the structure of **2**, the individual Fe–N$_{Me3TPyA}$ and Fe–N$_L$ distances are nearly identical, although the Fe–O distances range from 1.900(9) to 1.97(2) Å (see Table S1). While the different Fe–O distances indicate valence-trapping, the collective low variation in bond distances at the independent Fe sites suggests that the asymmetry of the structure may also partially arise due to crystal packing of the $[BAr^F_4]^-$ counteranions.

Table 2 summarizes the key comparisons in mean interatomic distances between the cationic complexes in **1** and **2**. In moving from **1** and **2**, the mean Fe–N$_{Me3TPyA}$ distance decreases by 2.5%, from 2.264(7) to 2.21(2) Å. In addition, the mean Fe–N$_L$ distance decreases by 5.2%, from 2.244(7) to 2.13(2) Å, and the Fe–O distance decreases by 1.5%, from 1.972(6) to 1.94(1) Å. These decreases in bond lengths at Fe upon oxidation are consistent with an oxidation of a single Fe center from Fe^{II} to Fe^{III}. In further support of this assignment, no statistically significant differences are observed for the C–C$_L$, N–C$_L$, or C–O bond distances. In sum, this structural comparison provides strong evidence that the oxidation of **1** to **2** involves a primarily metal-based redox event. Finally, the structure of **2** features a mean intramolecular Fe···Fe distance of 8.029(4) Å and a closest intermolecular Fe···Fe distance of 14.360(6) Å.

Mössbauer Spectroscopy. In order to confirm the presence of a metal-based oxidation and to probe the nature of mixed valency in $[(Me_3TPyA)_2Fe_2(L)]^{3+}$, Mössbauer spectra were collected for solid samples of **1** and **2** under zero applied field. At 5 and 80 K, the spectrum for **1** consists of a slightly broadened quadrupole doublet. Each of these spectra is best fit considering two symmetric quadrupole doublets with equal areas and line widths, consistent with the presence of two crystallographically inequivalent Fe centers, with an average isomer shift and quadrupole splitting of δ = 1.095(2) mm/s and ΔE_Q = 2.152(4) mm/s, respectively, and a line width of Γ = 0.270(3) mm/s (see Figure S2a and Table S2a). These parameters are typical of high-spin Fe^{II} and are close to those previously reported for diiminobenzoquinone- and azophenine-bridged Fe_2 complexes.[38,40]

The Mössbauer spectra for **2** were measured from 50 to 260 K and at 5 K (see Figure 3 upper and lower). The former spectra reveal a spectral profile as a function of temperature that is typical of a Class II/III mixed-valence, high-spin $Fe^{II}Fe^{III}$ complex that is undergoing relaxation as the result of electron hopping on the Mössbauer time scale of 10^{-8} s. The spectra from 50 to 260 K were fit with a model[41] involving relaxation between a high-spin Fe^{II} and a high-spin Fe^{III} quadrupole doublet (see Figure 3, upper, Figure S2b, and Table 3). Note that these fits are made difficult because of an absence of knowledge of the Fe^{II} and Fe^{III} doublet hyperfine parameters, first, in the slow relaxation limit that is unknown because of the onset of slow paramagnetic relaxation below ca. 40 to 50 K and,
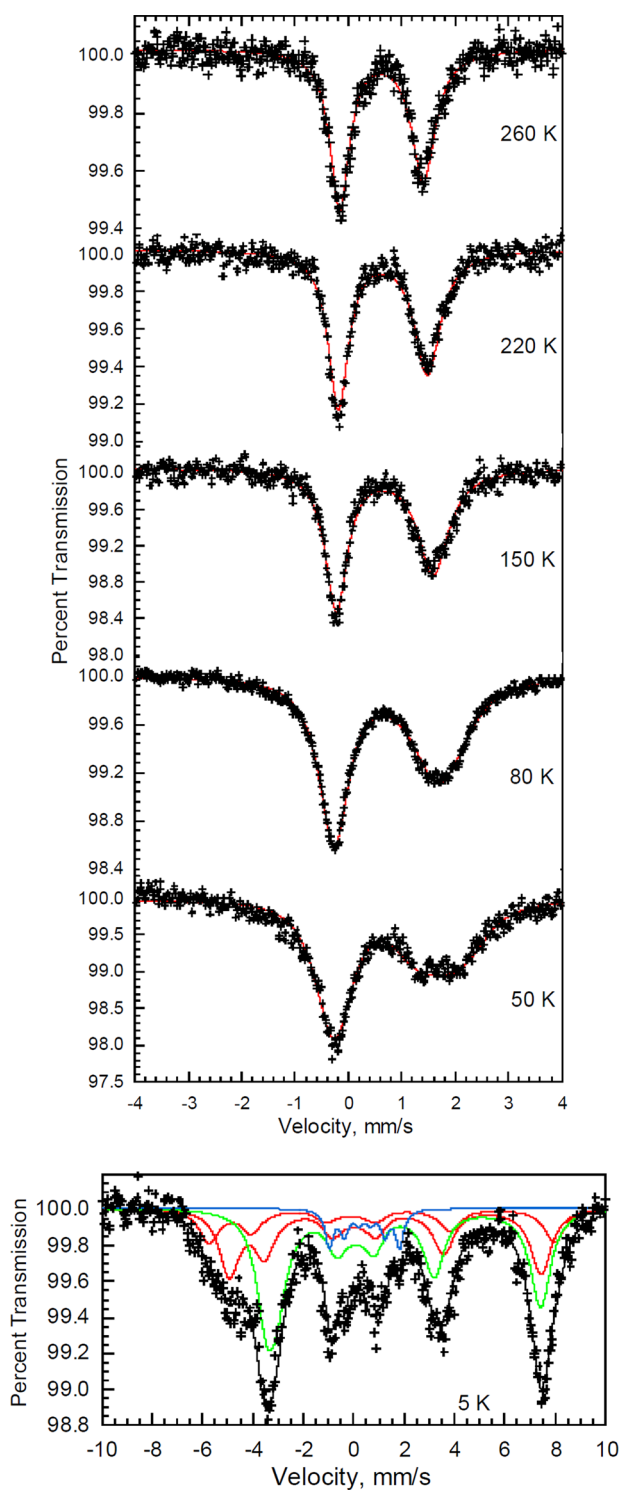
Figure 3. Upper: Mössbauer spectra for **2**, measured at the indicated temperatures between 50 and 260 K. Black crosses represent experimental data, and red lines correspond to fits considering electron hopping between Fe^{II} and Fe^{III}, as described in the text. Lower: 5 K Mössbauer spectrum for **2**. Green, red, and blue lines are fits corresponding to Fe^{II} sites, Fe^{III} sites, and an Fe^{III} impurity, respectively.

second, of the average $Fe^{II/III}$ doublet in the fast relaxation limit, presumably somewhat above ca. 300 K and unobtainable because of the thermal instability of **2** above ca. 260 K. Furthermore, it is difficult to surmise the best intrinsic line

width to use in the relaxation fits owing to the presence of three crystallographically distinct Fe_2 complexes in **2**, which involve electron hopping between Fe1···Fe1, Fe2···Fe2, and Fe3···Fe4, each of which may possibly have slightly different limiting hyperfine parameters. To overcome this difficulty, a $\Gamma = 0.40$ mm/s, the narrowest absorption observed near 0 mm/s at 220 K, was used to represent an upper limit of the intrinsic line width of the limiting quadrupole doublets.

Despite these difficulties, the observed spectral profiles are well fit considering an electron hopping mechanism (see Supporting Information for further details). The fits clearly reveal that both limiting quadrupole doublets must have the same sign of ΔE_Q, a sign that is most likely positive based on a fit of the 5 K spectrum discussed below. An Arrhenius plot of the logarithm of the electron hopping frequency, ν, yields an activation energy for the electron hopping of 63(8) cm^{-1}, a value that is consistent with the upper limit of activation energy obtained from optical spectroscopy (see Figure S2c).

The presence of a very asymmetric quadrupole doublet with decreasing temperature is indicative of an intervalence charge transfer, or electron hopping, between the Fe^{II} and Fe^{III} ions at a rate similar to that of the Mössbauer time scale. Similar behavior has been observed in $Fe^{II}Fe^{III}$-containing cationic biferrocene[42] and oxo-centered, carboxylato-bridged $Fe^{II}Fe^{III}_2$[43] complexes. Importantly, heat capacity measurements have shown that the onset of valence detrapping in these complexes usually stems from a phase transition involving intermolecular interactions, rather than simple thermal effects on the kinetics of electron hopping.[44] In these cases, the absence of any line broadening with changing temperature provided key evidence of such lattice effects. In contrast, the spectra of **2** unambiguously exhibit asymmetric line broadening with decreasing temperature as would be expected as the rate of electron hopping decreases with decreasing thermal energy. Moreover, to our knowledge, **2** represents the second example of a molecule with a high-spin ground state that exhibits changes in electron hopping rate observable by Mössbauer spectroscopy, which was first reported in a phenoxo-bridged $[Fe_2]^V$ complex with an $S = 9/2$ ground state.[45]

Below 50 K, the spectrum for **2** undergoes further broadening and splitting until broadened sextets indicative of slow paramagnetic relaxation are observed at 5 K (see Figure 3, lower). This behavior suggests that **2** is a single-molecule magnet at zero-field on the Mössbauer time scale (see below for further discussion of ac magnetic susceptibility measurements). Analysis of the 5 K Mössbauer spectrum of **2** is complicated because it requires at least three broadened sextets and, apparently, a small amount of Fe^{III} impurity. Nevertheless, the data can be modeled assuming that at 5 K **2** is a Class I mixed-valence complex with no electron hopping, but in which the Fe^{II} and Fe^{III} ion moments undergo $\pm z$ anisotropic slow paramagnetic relaxation with a frequency of 6.8(3) MHz, similar to the Larmor precession frequency (see Table S2b). More details of the analysis of the 5 K spectrum, along with the resulting fit parameters, are given in the Supporting Information.

UV–Vis–NIR Spectroscopy. To further probe the electronic structure of **1** and **2**, the UV–vis–NIR absorption spectra were collected for solution samples of **1** and **2** in CD_2Cl_2 at 298 K. The UV–vis–NIR spectrum for **1**, as depicted in Figure 4, exhibits an intense band at $\nu_{max} = 26737$ cm^{-1} with a shoulder at 27548 cm^{-1}. Considering the reduction of intensity upon oxidation (see below), we tentatively assign

Table 3. Mössbauer Spectral Parameters[a] for 2

T (K)	$\delta_{Fe(II)}$ (mm/s)[b]	$\Delta E_{Q,Fe(II)}$ (mm/s)	$\delta_{Fe(III)}$ (mm/s)[b]	$\Delta E_{Q,Fe(III)}$ (mm/s)	ν (MHz)	Area (% ε) (mm/s)
260	0.738(9)	2.39(2)	0.506(9)	0.74(2)	46(6)	0.75(1)
220	0.783(7)	2.58(1)	0.515(7)	0.75(2)	43(3)	1.19(1)
150	0.820(5)	2.89(1)	0.546(4)	0.74(1)	38(1)	2.40(3)
115	0.845(5)	3.00(1)	0.551(4)	0.77(1)	30(1)	3.40(3)
80	0.861(4)	3.15(1)	0.576(4)	0.80(1)	18.0(3)	3.85(1)
50	0.880(7)	3.17(2)	0.570(8)	0.81(2)	11.4(3)	4.12(5)

[a]Statistical fitting errors are given in parentheses. The actual errors may be two to three times as large. The iron(II) to iron(III) area ratio was fixed to 1:1 and the line width to 0.40 mm/s. [b]The isomer shifts are reported relative to α-iron foil measured at 295 K.
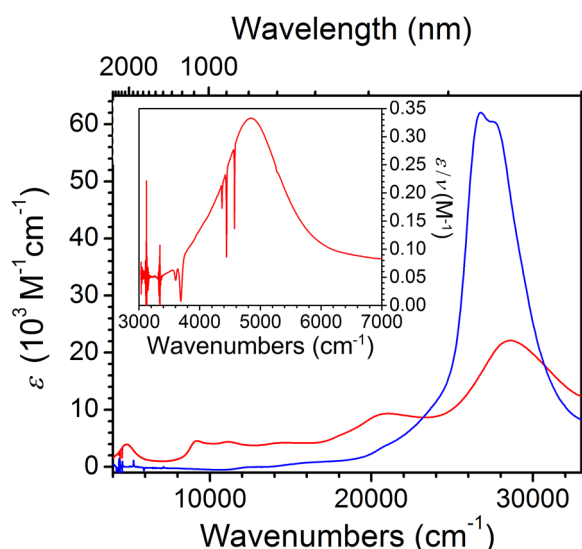

Figure 4. UV–vis–NIR spectra for CD_2Cl_2 solutions of **1** (blue) and **2** (red). Inset: Expanded view of the NIR region for **2**.

these features to metal-to-ligand charge transfer (MLCT) transitions. The sharp peaks in the low energy region likely correspond to vibronic overtones of CH_2Cl_2 impurities in the solvent that are too intense for an accurate background subtraction.

The spectrum obtained for **2** exhibits a markedly different profile than that of **1**. The MLCT bands broaden and decrease in intensity, with the maximum shifted to ν_{max} = 28409 cm^{-1}. Additionally, new bands appear at ν_{max} = 20703, 13986, 10952, and 4810 cm^{-1}. Of the new bands, we assign the lowest energy feature, positioned in the NIR region with a molar absorption coefficient of ε_{max} = 3950 M^{-1} cm^{-1}, to an intervalence charge transfer (IVCT) band. This feature exhibits a bandwidth of $\Delta\nu_{1/2}$ = 1403 cm^{-1}, which is much lower than the theoretical bandwidth of $\nu^{\circ}_{1/2}$ = $(2310(\nu_{max}))^{1/2}$ = 3333 cm^{-1} obtained considering a classical two-state model.[46] Accordingly, this result suggests the presence of at least some degree of valence detrapping in the mixed-valence compound **2**. Further, the ratio between the experimental and the theoretical bandwidth gives the parameter $\Gamma = 1 - \nu_{1/2}/\nu^{\circ}_{1/2}$ = 0.58, which is close to the value of Γ = 0.50 expected at the Class II-Class III transition.[47] Moreover, the relatively symmetric shape of the IVCT band lacks a cutoff on the lower energy side that is commonly observed in delocalized, Class III mixed-valence compounds (see Figure 4, inset).[48] Taken together with the variable-temperature Mössbauer spectra and crystal structure, these results suggest that **2** may be best described as a Class II–III mixed-valence compound.[49] Note that an examination of the solvent dependence of the IVCT transition was precluded due

to the low stability of **2** in other solvents that have high transparency in the NIR region. Nevertheless, the solid-state spectrum of **2** was investigated by diffuse reflectance spectroscopy (see Figure S3). Although the detector limit did not allow full analysis of the IVCT band, the position and relative intensity of the NIR features are similar to those observed in solution.

To quantify the extent of electronic coupling and the energy of activation, the IVCT band was further analyzed. In the case of a delocalized Class III system, the electronic coupling parameter, is given as H_{AB} = $0.5\nu_{max}$ = 2405 cm^{-1}, which provides an upper limit of the coupling. Alternatively, H_{AB} may be calculated using the classical two-site model considering the electron transfer distance in Å, r_{AB},[48a,49,50] which gives H_{AB} = 419 cm^{-1} in the case of **2**. Here, the value of H_{AB} represents a lower bound, as the electron transfer distance in the presence of significant electronic mixing with the ligand orbitals and/or between metal centers across the ligand can be considerably shorter than the geometrical distances obtained from the structural analysis. Furthermore, the energies of the thermal and optical processes are directly related, and the activation energy for thermal electron transfer in a Class II system is given as $E_a = \nu_{max}/4 - H_{AB} + H_{AB}^2/\nu_{max}$ = 820 cm^{-1}.[46] As the value of H_{AB} = 419 cm^{-1} represents the lower limit of electronic coupling, the true value of E_a in **2** should be smaller than 820 cm^{-1}, which is consistent with the observation of a thermally activated transition from a trapped to detrapped valence in the Mössbauer spectra.

The double exchange parameter B can also be extracted from the IVCT band. In the case of a delocalized Class III system, the most intense energy of the IVCT transition, ν_{max}, is equated with the spin state transition in the ground state, $10B$.[51] This gives a double exchange parameter of B = 481 cm^{-1} for **2**, which is nearly seven times larger than that extracted from the magnetic data (see below). The observed discrepancy arises because this analysis assumes full electronic delocalization and neglects vibronic coupling and the role of the bridging ligand. Finally, note that the classical two-state theory cannot adequately describe electronic exchange for compounds near the Class II-Class III transition, and as such a complete understanding of the electronic structure of **2** requires a detailed theoretical analysis that is beyond the scope of this work.

Static Magnetic Properties. To assess potential magnetic interactions in **1** and **2**, variable-temperature dc magnetic susceptibility data were collected for solid samples under an applied field of 1 T. The resulting plots of $\chi_M T$ vs T for both compounds are shown in Figure 5. In the case of **1**, $\chi_M T$ = 6.65 cm^3 K mol^{-1} at 300 K, corresponding to two magnetically isolated S = 2 Fe^{II} centers with g = 2.08. As the temperature is decreased, the value of $\chi_M T$ increases gradually down to 100 K
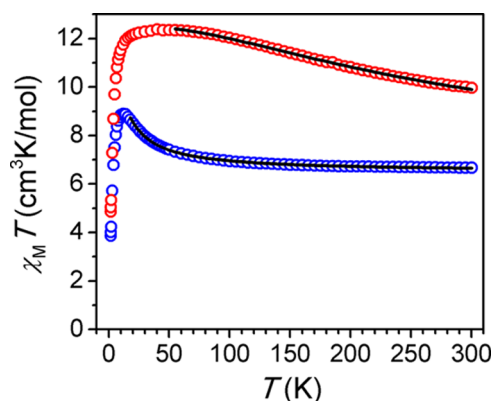
Figure 5. Variable-temperature dc magnetic susceptibility data for **1** (blue) and **2** (red), collected under an applied field of 1 T. The black lines correspond to fits of the data.

and then more steeply, reaching a maximum value of 8.9 cm^3 K mol^{-1} at 12 K. This increase in $\chi_M T$ with decreasing temperature indicates weak ferromagnetic superexchange coupling between high-spin Fe^{II} centers through the diamagnetic bridging ligand, resulting in an $S = 4$ ground state. Below 12 K, $\chi_M T$ decreases sharply to a value of 3.86 cm^3 K mol^{-1} at 1.8 K, stemming from Zeeman splitting, zero-field splitting, and potentially weak intermolecular interactions. In order to quantify the ferromagnetic superexchange in **1**, the data were fit in the temperature range 18−300 K to the Van Vleck equation according to the spin Hamiltonian $\hat{H} = -2J(\hat{S}_{Fe1} \cdot \hat{S}_{Fe2})$, giving an exchange constant of $J = +1.21(1)$ cm^{-1} and $g = 2.08(1)$. Here, the magnitude of J is consistent with other examples of benzoquinonoid-bridged Fe$^{II}_2$ complexes. More specifically, $|J|$ is larger than that of 0.70 cm^{-1} reported for a tetraoxolene-bridged complex,[52] but smaller than that of 2.90(2) cm^{-1} reported for a tetraazalene-bridged complex.[40] This intermediate value is expected, given the presence of two hydroxo and two imino donors on the bridging ligand of **1**. Finally, low-temperature magnetization data collected for **1** confirm the presence of an $S = 4$ ground state, with a fit to the data giving parameters of $D = -4.9$ cm^{-1} and $g = 2.1$ (see Figure S4).

In contrast, the plot of $\chi_M T$ vs T for **2** exhibits a markedly different profile. The value of $\chi_M T$ at 300 K of 9.97 cm^3 K mol^{-1} is considerably higher than that expected for isolated $S = 2$ Fe^{II} and $S = {}^5/_2$ Fe^{III} centers with $g = 2.00$. As the temperature is decreased, $\chi_M T$ undergoes a nearly monotonic increase to reach a maximum value of 12.38 cm^3 K mol^{-1} at 40 K, very close to that expected for exclusive population of an $S = {}^9/_2$ ground state. Indeed, low-temperature magnetization data confirm this ground state, with a fit to the data giving parameters of $D = +3.4$ cm^{-1} and $g = 2.1$ (see Figure S5).[53] Considering the evidence for electron hopping in **2**, as ascertained from Mössbauer and UV−vis−NIR spectra, the data were modeled using the Van Vleck equation according to the Hamiltonian $\hat{H} = -2J(\hat{S}_{Fe1} \cdot \hat{S}_{Fe2} \hat{O}_{Fe1} + \hat{S}_{Fe1} \cdot \hat{S}_{Fe2} \hat{O}_{Fe2}) + BT_{Fe1Fe2}$, where J and B are the Heisenberg and double-exchange constants, respectively.[54] Accordingly, fits to the data in the temperature range 65−300 K give values of $J = +8.9(7)$ cm^{-1}, $B = 69(4)$ cm^{-1}, and $g = 2.01(1)$. Note that small changes to the low-temperature limit of data included in fitting leads to large variation in J and B, likely owing to the lack of significant temperature dependence of the $\chi_M T$ vs T data. Moreover, these parameters represent the average values of the

three crystallographically distinct intramolecular Fe···Fe distances. As such, these values should be regarded as estimates. Below 50 K, the data undergo a sharp downturn as a result of zero-field and Zeeman splitting.

The value of $B = 69(4)$ cm^{-1} obtained for **2** is smaller than those previously reported in other double-exchange complexes. Previously reported mixed-valence [Fe$_2$]^V complexes exhibit values of $B = 943$[14a]-1320[13b] cm^{-1}, while a [V$_2$]^V complex was shown to feature a double exchange parameter of $B = 122$ cm^{-1}.[18,55] This difference likely stems in part from the large intramolecular Fe···Fe distance of 8.029(4) Å in **2**, compared to those of 2.509(6)[13b]−2.7485(5)[15] Å and 6.188 Å[18] previously observed in the [Fe$_2$]^V complexes and [V$_2$]^V complex noted above, respectively. Indeed, to the best of our knowledge, **2** features the largest intramolecular metal−metal separation yet observed in a complex that exhibits a double-exchange mechanism, although we note that a radical−radical separation of ca. 22 Å has been observed for an $S = {}^3/_2$ organic molecule with electron delocalization between two nitronyl nitroxide centers mediated through a bridging Co^{III} bis(semiquinonate) unit.[56] Nevertheless, the present result demonstrates the ability of quinonoid bridging ligands to mediate electron hopping through double-exchange coupling between high-spin metal centers.

Dynamic Magnetic Properties. Finally, in order to probe for slow magnetic relaxation in **1** and **2**, variable-frequency ac magnetic susceptibility data were collected on solid samples. Under zero applied dc field, neither compound exhibits slow magnetic relaxation above 1.8 K and below 1500 Hz. However, upon application of a 750 Oe dc field, which provides the slowest dynamics as confirmed by field dependence of variable-frequency ac susceptibility data (see Figure S6), temperature-dependent features are observed for **1** in the plot of χ_M'' vs ν (see Figure 6). These isotherms were used to construct Cole−Cole plots, which were fit considering a generalized Debye model to extract a relaxation time at each temperature (see Figures S7 and S8).[32] As depicted in the inset of Figure 6, the relaxation time of **2** exhibits thermally activated behavior at high temperature, with a linear fit to the data in the temperature range 2.2−2.4 K providing a relaxation barrier of 14(1) cm^{-1}. Note that, owing to the weak intramolecular Fe···Fe exchange of $J = +1.21(1)$ cm^{-1} in **1**, this slow relaxation may involve spin excited states in addition to the $S = 4$ ground state.
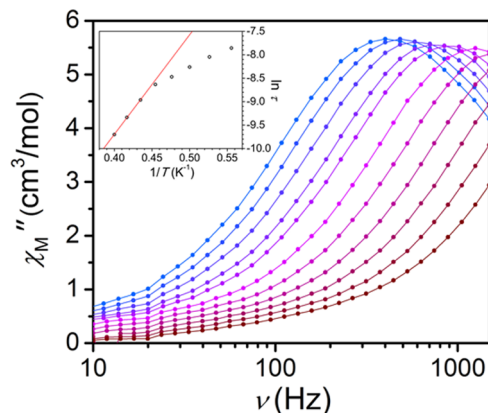
Figure 6. Variable-frequency ac susceptibility data for **1**, collected under an applied dc field of 750 Oe in the temperature range 1.8 (blue) to 2.7 (red) K. Inset: Arrhenius plot of relaxation time, with a linear fit giving $U_{eff} = 14(1)$ cm^{-1}.

Under an applied dc field of 750 Oe, **2** exhibits only tails at high frequency above 1.8 K, and therefore features a much smaller relaxation barrier than **1** (see Figure S9). Accordingly, the complex $[(Me_3TPyA)_2Fe^{II}_2(L)]^{n+}$ can be described as a redox-switchable single-molecule magnet, where one-electron redox chemistry can be employed to significantly modulate magnetic relaxation time. To date, very few redox-switchable single-molecule magnets have been reported,[57] including a cyano-bridged Mn_4Re cluster,[58] a nindigo-bridged Co_2 complex,[59] and an azophenine-bridged Fe_2 complex.[40] This class of molecules could find use in devices such as single-molecule transistors, where a gate voltage can be used to reversibly switch spin state and relaxation dynamics.[60] Interestingly, the presence of tails in the plot of χ_M'' vs ν for **2** suggests slow magnetic relaxation, albeit corresponding to a miniscule relaxation barrier, in spite of a positive D value extracted from magnetization data. As fitting magnetization data is often an unreliable method for obtaining the sign of zero-field splitting parameters, we cannot rule out the possibility that D is in fact negative. Nevertheless, recent work has uncovered a number of single-molecule magnets with positive D values confirmed by high-field EPR measurements.[4c,61]

The presence of slow magnetic relaxation in **2** is consistent with the Mössbauer spectra presented above, which reveal slow paramagnetic relaxation at 5 K even at zero field, because Mössbauer spectroscopy probes a much faster time scale, and therefore higher temperature range, than ac magnetic susceptibility. As such, we hypothesize that fast relaxation processes, such as quantum tunneling or spin−spin relaxation, are operative in **2** at the low temperatures probed by ac susceptibility. Indeed, a similar phenomenon, where slow magnetic relaxation is evident from zero-field Mössbauer spectra but only from ac susceptibility under an applied dc field, has been reported in mononuclear trigonal pyramidal[62] and linear, two-coordinate[63] Fe^{II} complexes.

SUMMARY AND OUTLOOK

The foregoing results demonstrate that quinonoid bridging ligands can mediate electron hopping between metal centers through a double-exchange mechanism in mixed-valence Fe_2 complexes, as exemplified in the $S = ^9/_2$ complex $[(Me_3TPyA)_2Fe_2(L)]^{3+}$, thereby providing the first example of double-exchange through an organic ligand between Fe centers. Accordingly, variable-temperature dc magnetic susceptibility data can be modeled considering double-exchange, with a fit to the data providing values of $J = +8.9(7)$ cm^{-1} and $B = 69(4)$ cm^{-1}. Moreover, variable-temperature Mössbauer spectra for this complex reveal a thermally induced transition from a valence-trapped to detrapped state, with an activation energy for electron hopping of $63(8)$ cm^{-1}. Finally, while the mixed-valence complex exhibits only tails in the ac magnetic susceptibility, a corresponding one electron-reduced Fe^{II}_2 complex displays single-molecule magnet behavior with a relaxation barrier of $U_{eff} = 14(1)$ cm^{-1}. Work is underway to elucidate the role of benzoquinone substitution in governing double-exchange and to incorporate benzoquinone bridges into mixed-valence extended solids.

ASSOCIATED CONTENT

Ⓢ Supporting Information

The Supporting Information is available free of charge on the ACS Publications website at DOI: 10.1021/jacs.5b07251.

NMR spectra for **1** and **2**, additional structural information for **2**, additional Mössbauer spectra and details of analysis, and additional magnetic data for **1** and **2**. (PDF)

Crystallographic information file for **1**. (CIF)

Crystallographic information file for **2**. (CIF)

AUTHOR INFORMATION

Corresponding Author
*dharris@northwestern.edu

Present Address
§Department of Chemistry, University of Chicago, Chicago, Illinois 60637, United States.

Notes
The authors declare no competing financial interest.

ACKNOWLEDGMENTS

REFERENCES

(1) (a) Gatteschi, D.; Sessoli, R.; Villain, J. *Molecular Nanomagnets*; Oxford University Press: Oxford, 2006. (b) Winpenny, R. E. P. *Single Molecule Magnets and Related Phenomena*; Springer: Berlin, 2006; Vol. 122.

(2) (a) Leuenberger, M. N.; Loss, D. *Nature* **2001**, *410*, 789. (b) Rocha, A. R.; García-Suárez, V. M.; Bailey, S. W.; Lambert, C. J.; Ferrer, J.; Sanvito, S. *Nat. Mater.* **2005**, *4*, 335. (c) Bogani, L.; Wernsdorfer, W. *Nat. Mater.* **2008**, *7*, 179. (d) Stamp, P. C. E.; Gaita-Arino, A. *J. Mater. Chem.* **2009**, *19*, 1718. (e) Ardavan, A.; Blundell, S. J. *J. Mater. Chem.* **2009**, *19*, 1754.

(3) Multinuclear complexes: (a) Caneschi, A.; Gatteschi, D.; Sessoli, R.; Barra, A. L.; Brunel, L. C.; Guillot, M. *J. Am. Chem. Soc.* **1991**, *113*, 5873. (b) Sessoli, R.; Tsai, H.-L.; Schake, A. R.; Wang, J. B.; Folting, K.; Gatteschi, D.; Christou, G.; Hendrickson, D. N. *J. Am. Chem. Soc.* **1993**, *115*, 1804. (c) Sessoli, R.; Gatteschi, D.; Caneschi, A.; Novak, M. A. *Nature* **1993**, *365*, 141. (d) Sokol, J. J.; Hee, A. G.; Long, J. R. *J. Am. Chem. Soc.* **2002**, *124*, 7656. (e) Berlinguette, C. P.; Vaughn, D.; Cañada-Vilalta, C.; Galán-Mascarós, J. R.; Dunbar, K. R. *Angew. Chem., Int. Ed.* **2003**, *42*, 1523. (f) Parsons, S.; Perlepes, S. P.; Christou, G.; Brechin, E. K. *J. Am. Chem. Soc.* **2007**, *129*, 2754. (g) Bagai, R.; Christou, G. *Chem. Soc. Rev.* **2009**, *38*, 1011.

(4) Mononuclear complexes: (a) Freedman, D. E.; Harman, W. H.; Harris, T. D.; Long, G. J.; Chang, C. J.; Long, J. R. *J. Am. Chem. Soc.* **2010**, *132*, 1224. (b) Zadrozny, J. M.; Long, J. R. *J. Am. Chem. Soc.* **2011**, *133*, 20732. (c) Craig, G. A.; Murrie, M. *Chem. Soc. Rev.* **2015**, *44*, 2135.

(5) Multinuclear complexes: (a) Tang, J.; Hewitt, I. J.; Madhu, N. T.; Chastanet, G.; Wernsdorfer, W.; Anson, C. E.; Benelli, C.; Sessoli, R.; Powell, A. K. *Angew. Chem., Int. Ed.* **2006**, *45*, 1729. (b) Lin, P.-H.; Burchell, T. J.; Clérac, R.; Murugesu, M. *Angew. Chem., Int. Ed.* **2008**, *47*, 8848. (c) Rinehart, J. D.; Fang, M.; Evans, W. J.; Long, J. R. *J. Am. Chem. Soc.* **2011**, *133*, 14236.

(6) Mononuclear complexes: (a) Ishikawa, N.; Sugita, M.; Ishikawa, T.; Koshihara, S.-y.; Kaizu, Y. *J. Am. Chem. Soc.* **2003**, *125*, 8694. (b) AlDamen, M. A.; Clemente-Juan, J. M.; Coronado, E.; Marti-Gastaldo, C.; Gaita-Ariño, A. *J. Am. Chem. Soc.* **2008**, *130*, 8874. (c) Rinehart, J. D.; Long, J. R. *Chem. Sci.* **2011**, *2*, 2078. (d) Ganivet, C. R.; Ballesteros, B.; de la Torre, G.; Clemente-Juan, J. M.; Coronado,

E.; Torres, T. *Chem. - Eur. J.* **2013**, *19*, 1457. (e) Liddle, S. T.; van Slageren, J. *Chem. Soc. Rev.* **2015**, *44*, 6655.

(7) Multinuclear complexes: (a) Magnani, N.; Colineau, E.; Eloirdi, R.; Griveau, J. C.; Caciuffo, R.; Cornet, S. M.; May, I.; Sharrad, C. A.; Collison, D.; Winpenny, R. E. P. *Phys. Rev. Lett.* **2010**, *104*, 197202. (b) Mills, D. P.; Moro, F.; McMaster, J.; van Slageren, J.; Lewis, W.; Blake, A. J.; Liddle, S. T. *Nat. Chem.* **2011**, *3*, 454.

(8) Mononuclear complexes: (a) Rinehart, J. D.; Long, J. R. *J. Am. Chem. Soc.* **2009**, *131*, 12558. (b) Magnani, N.; Apostolidis, C.; Morgenstern, A.; Colineau, E.; Griveau, J.-C.; Bolvin, H.; Walter, O.; Caciuffo, R. *Angew. Chem., Int. Ed.* **2011**, *50*, 1696.

(9) (a) Kahn, O. *Molecular Magnetism*; VCH: New York, 1993. (b) Demir, S.; Jeon, I.-R.; Long, J. R.; Harris, T. D. *Coord. Chem. Rev.* **2015**, *289*, 149.

(10) (a) Coulon, C.; Miyasaka, H.; Clérac, R. *Struct. Bonding (Berlin)* **2006**, *122*, 163. (b) Feng, X.; Harris, T. D.; Long, J. R. *Chem. Sci.* **2011**, *2*, 1688. (c) Gatteschi, D. In *Molecular Magnets*; Bartolomé, J., Luis, F., Fernández, J., Eds.; Springer-Verlag: Berlin, 2014; Vol. *1*, p 191. (d) Coulon, C.; Pianet, V.; Urdampilleta, M.; Clérac, R. *Struct. Bonding (Berlin, Ger.)* **2014**, *164*, 143.

(11) Domb, C. In *Phase Transition and Critical Phenomena*; Domb, C.; Green, M. S., Eds.; Academic Press: London, NY, 1974; Vol. 3, Chapter 6, p 357.

(12) (a) Zener, C. *Phys. Rev.* **1951**, *82*, 403. (b) Girerd, J.-J. *J. Chem. Phys.* **1983**, *79*, 1766.

(13) (a) Drüeke, S.; Chaudhuri, P.; Pohl, K.; Wieghardt, K.; Ding, X.-Q.; Bill, E.; Sawaryn, A.; Trautwein, A. X.; Winkler, H.; Gurman, S. J. *J. Chem. Soc., Chem. Commun.* **1989**, 59. (b) Gamelin, D. R.; Bominaar, E. L.; Kirk, M. L.; Wieghardt, K.; Solomon, E. I. *J. Am. Chem. Soc.* **1996**, *118*, 8085.

(14) (a) Dutta, S. K.; Ensling, J.; Werner, R.; Flörke, U.; Haase, W.; Gütlich, P.; Nag, K. *Angew. Chem., Int. Ed. Engl.* **1997**, *36*, 152. (b) Hazra, S.; Sasmal, S.; Fleck, M.; Grandjean, F.; Sougrati, M. T.; Ghosh, M.; Harris, T. D.; Bonville, P.; Long, G. J.; Mohanta, S. *J. Chem. Phys.* **2011**, *134*, 174507.

(15) Hagadorn, J. R.; Que, L., Jr.; Tolman, W. B.; Prisecaru, I.; Münck, E. *J. Am. Chem. Soc.* **1999**, *121*, 9760.

(16) (a) Lee, D.; Krebs, C.; Huynh, B. H.; Hendrich, M. P.; Lippard, S. J. *J. Am. Chem. Soc.* **2000**, *122*, 5000. (b) Lee, D.; DuBois, J. L.; Pierce, B.; Hedman, B.; Hodgson, K. O.; Hendrich, M. P.; Lippard, S. J. *Inorg. Chem.* **2002**, *41*, 3172.

(17) (a) Noodleman, L.; Baerends, E. J. *J. Am. Chem. Soc.* **1984**, *106*, 2316. (b) Münck, E.; Papaefthymiou, V.; Surerus, K. K.; Girerd, J.-J. *Metal Clusters in Proteins*; Que, L., Jr., Ed.; American Chemical Society: Washington, D.C., 1988; pp 302−325. (c) Noodleman, L.; Case, D. A. *Adv. Inorg. Chem.* **1992**, *38*, 423. (d) Borshch, S. A.; Bominaar, E. L.; Blondin, G.; Girerd, J.-J. *J. Am. Chem. Soc.* **1993**, *115*, 5155. (e) Achim, C.; Golinelli, M.-P.; Bominaar, E. L.; Meyer, J.; Münck, E. *J. Am. Chem. Soc.* **1996**, *118*, 8168.

(18) Bechlars, B.; D'Alessandro, D. M.; Jenkins, D. J.; Iavarone, A. T.; Glover, S. D.; Kubiak, C. P.; Long, J. R. *Nat. Chem.* **2010**, *2*, 362.

(19) Co: Heinze, K.; Huttner, G.; Walter, O. *Eur. J. Inorg. Chem.* **1999**, *1999*, 593.

(20) Ni: Siri, O.; Taquet, J. P.; Collin, J. P.; Rohmer, M. M.; Bénard, M.; Braunstein, P. *Chem. - Eur. J.* **2005**, *11*, 7247.

(21) Ru: (a) Kar, S.; Sarkar, B.; Ghumaan, S.; Janardanan, D.; van Slageren, J.; Fiedler, J.; Puranik, V. G.; Sunoj, R. B.; Kaim, W.; Lahiri, G. K. *Chem. - Eur. J.* **2005**, *11*, 4901. (b) Ghumaan, S.; Sarkar, B.; Maji, S.; Puranik, V. G.; Fiedler, J.; Urbanos, F. A.; Jimenez-Aparicio, R.; Kaim, W.; Lahiri, G. K. *Chem. - Eur. J.* **2008**, *14*, 10816. (c) Das, H. S.; Das, A. K.; Pattacini, R.; Hübner, R.; Sarkar, B.; Braunstein, P. *Chem. Commun.* **2009**, 4387. (d) Das, H. S.; Weisser, F.; Schweinfurth, D.; Su, C. Y.; Bogani, L.; Fiedler, J.; Sarkar, B. *Chem. - Eur. J.* **2010**, *16*, 2977. (e) Weisser, F.; Huebner, R.; Schweinfurth, D.; Sarkar, B. *Chem. - Eur. J.* **2011**, *17*, 5727. (f) Sommer, M. G.; Schweinfurth, D.; Weisser, F.; Hohloch, S.; Sarkar, B. *Organometallics* **2013**, *32*, 2069. (g) Das, H. S.; Schweinfurth, D.; Fiedler, J.; Khusniyarov, M. M.; Mobin, S. M.; Sarkar, B. *Chem. - Eur. J.* **2014**, *20*, 4334. (h) Sarkar, B.; Schweinfurth, D.; Deibel, N.; Weisser, F. *Coord. Chem. Rev.* **2015**, *293*, 250.

(22) Os: Gupta, P.; Das, A.; Basuli, F.; Castineiras, A.; Sheldrick, W. S.; Mayer-Figge, H.; Bhattacharya, S. *Inorg. Chem.* **2005**, *44*, 2081.

(23) Buschmann, W. E.; Miller, J. S. *Chem. - Eur. J.* **1998**, *4*, 1731.

(24) Rosokha, S. V.; Stern, C. L.; Ritzert, J. T. *CrystEngComm* **2013**, *15*, 10638.

(25) Beni, A.; Dei, A.; Laschi, S.; Rizzitano, M.; Sorace, L. *Chem. - Eur. J.* **2008**, *14*, 1804.

(26) Amonoo-Neizer, E. H.; Shaw, R. A.; Skovlin, D. O.; Smith, B. C. *Inorg. Synth.* **1966**, *8*, 19.

(27) *SAINT: Software for the Integration of CCD Detector System*, version 8.27B; Bruker AXS Inc.: Madison, WI, 2007.

(28) Sheldrick, G. M. *Acta Crystallogr., Sect. A: Found. Adv.* **2015**, *71*, 3.

(29) Sheldrick, G. M. *Acta Crystallogr., Sect. A: Found. Crystallogr.* **2008**, *64*, 112.

(30) Dolomanov, O. V.; Bourhis, L. J.; Gildea, R. J.; Howard, J. A. K.; Puschmann, H. *J. Appl. Crystallogr.* **2009**, *42*, 339.

(31) Thorn, A.; Dittrich, B.; Sheldrick, G. M. *Acta Crystallogr., Sect. A: Found. Crystallogr.* **2012**, *68*, 448.

(32) (a) Cole, K. S.; Cole, R. H. *J. Chem. Phys.* **1941**, *9*, 341. (b) Boettcher, C. J. F. *Theory of Electric Polarisation*; Elsevier: Amsterdam, 1952. (c) Aubin, S. M.; Sun, Z.; Pardi, L.; Krzysteck, J.; Folting, K.; Brunel, L.-J.; Rheingold, A. L.; Christou, G.; Hendrickson, D. N. *Inorg. Chem.* **1999**, *38*, 5329.

(33) Bain, G. A.; Berry, J. F. *J. Chem. Educ.* **2008**, *85*, 532.

(34) (a) Das, H. S.; Weisser, F.; Schweinfurth, D.; Su, C.-Y.; Bogani, L.; Fiedler, J.; Sarkar, B. *Chem. - Eur. J.* **2010**, *16*, 2977. (b) Sommer, M. G.; Schweinfurth, D.; Weisser, F.; Hohloch, S.; Sarkar, B. *Organometallics* **2013**, *32*, 2069. (c) Das, H. S.; Schweinfurth, D.; Fiedler, J.; Khusniyarov, M. M.; Mobin, S. M.; Sarkar, B. *Chem. - Eur. J.* **2014**, *20*, 4334.

(35) (a) Schweinfurth, D.; Khusniyarov, M. M.; Bubrin, D.; Hohloch, S.; Su, C.-Y.; Sarkar, B. *Inorg. Chem.* **2013**, *52*, 10332. (b) Schweinfurth, D.; Rechkemmer, Y.; Hohloch, S.; Deibel, N.; Peremykin, I.; Fiedler, J.; Marx, R.; Neugebauer, P.; van Slageren, J.; Sarkar, B. *Chem. - Eur. J.* **2014**, *20*, 3475.

(36) Zhang, D.; Jin, G.-X. *Organometallics* **2003**, *22*, 2851.

(37) Jia, W.-G.; Han, Y.-F.; Lin, Y.-J.; Weng, L.-H.; Jin, G.-X. *Organometallics* **2009**, *28*, 3459.

(38) Park, J. G.; Jeon, I.-R.; Harris, T. D. *Inorg. Chem.* **2015**, *54*, 359.

(39) Connelly, N. G.; Geiger, W. E. *Chem. Rev.* **1996**, *96*, 877.

(40) Jeon, I.-R.; Park, J. G.; Xiao, D. J.; Harris, T. D. *J. Am. Chem. Soc.* **2013**, *135*, 16845.

(41) (a) Litterst, F. J.; Amthauer, G. *Phys. Chem. Miner.* **1984**, *10*, 250. (b) Tjon, J. A.; Blume, M. *Phys. Rev.* **1968**, *165*, 456.

(42) (a) Dong, T.-Y.; Cohn, M. J.; Hendrickson, D. N.; Pierpont, C. G. *J. Am. Chem. Soc.* **1985**, *107*, 4777. (b) Cohn, M. J.; Dong, T.-Y.; Hendrickson, D. N.; Geib, S. J.; Rheingold, A. L. *J. Chem. Soc., Chem. Commun.* **1985**, 1095. (c) Dong, T.-Y.; Hendrickson, D. N.; Iwai, K.; Cohn, M. J.; Rheingold, A. L.; Sano, H.; Motoyama, I.; Nakashima, S. *J. Am. Chem. Soc.* **1985**, *107*, 7996. (d) Moore, M. F.; Wilson, S. R.; Cohn, M. J.; Dong, T.-Y.; Mueller-Westerhoff, U. T.; Hendrickson, D. N. *Inorg. Chem.* **1985**, *24*, 4559. (e) Dong, T.-Y.; Hendrickson, D. N.; Pierpont, C. G.; Moore, M. F. *J. Am. Chem. Soc.* **1986**, *108*, 963. (f) Dong, T. Y.; Kambara, T.; Hendrickson, D. N. *J. Am. Chem. Soc.* **1986**, *108*, 5857. (g) Dong, T. Y.; Schei, C. C.; Hsu, T. L.; Lee, S. L.; Li, S. J. *Inorg. Chem.* **1991**, *30*, 2457. (h) Manago, T.; Hayami, S.; Oshio, H.; Osaki, S.; Hasuyama, H.; Herber, R. H.; Maeda, Y. *J. Chem. Soc., Dalton Trans.* **1999**, 1001. (i) Oda, T.; Nakashima, S.; Okuda, T. *Bull. Chem. Soc. Jpn.* **2003**, *76*, 2129. (j) Venkatasubbaiah, K.; Doshi, A.; Nowik, I.; Herber, R. H.; Rheingold, A. L.; Jäkle, F. *Chem. - Eur. J.* **2008**, *14*, 444.

(43) (a) Cannon, R. D.; Montri, L.; Brown, D. B.; Marshall, K. M.; Elliott, C. M. *J. Am. Chem. Soc.* **1984**, *106*, 2591. (b) Oh, S. M.; Hendrickson, D. N.; Hassett, K. L.; Davis, R. E. *J. Am. Chem. Soc.* **1984**, *106*, 7984. (c) Oh, S. M.; Hendrickson, D. N.; Hassett, K. L.; Davis, R. E. *J. Am. Chem. Soc.* **1985**, *107*, 8009. (d) Sorai, M.; Kaji, K.; Hendrickson, D. N.; Oh, S. M. *J. Am. Chem. Soc.* **1986**, *108*, 702. (e) Woehler, S. E.; Wittebort, R. J.; Oh, S. M.; Kambara, T.;

Hendrickson, D. N.; Inniss, D.; Strouse, C. E. *J. Am. Chem. Soc.* **1987**, *109*, 1063. (f) Cannon, R. D.; White, R. P. *Prog. Inorg. Chem.* **1988**, *36*, 195. (g) Kaneko, Y.; Nakano, M.; Sorai, M.; Jang, H. G.; Hendrickson, D. N. *Inorg. Chem.* **1989**, *28*, 1067. (h) Jang, H. G.; Geib, S. J.; Kaneko, Y.; Nakano, M.; Sorai, M.; Rheingold, A. L.; Montez, B.; Hendrickson, D. N. *J. Am. Chem. Soc.* **1989**, *111*, 173. (i) Cannon, R. D.; Jayasooria, U. A.; Arap Koske, S. K.; White, R. P.; Williams, J. H. *J. Am. Chem. Soc.* **1991**, *113*, 4158. (j) Nakamoto, T.; Katada, M.; Kawata, S.; Kitagawa, S.; Kikuchi, K.; Ikemoto, I.; Endo, K.; Sano, H. *Chem. Lett.* **1993**, *22*, 1463. (k) Nakamoto, T.; Katada, M.; Kawata, S.; Kitagawa, S.; Sano, H.; Konno, M. *Hyperfine Interact.* **1994**, *93*, 1567. (l) Sato, T.; Ambe, F.; Endo, K.; Katada, M.; Maeda, H.; Nakamoto, T.; Sano, H. *J. Am. Chem. Soc.* **1996**, *118*, 3450. (m) Onaka, S.; Sakai, Y.; Ozeki, T.; Nakamoto, T.; Kobayashi, Y.; Takahashi, M.; Ogiso, R.; Takayama, T.; Shiotsuka, M. *Dalton Trans.* **2014**, *43*, 6711. (n) Okazawa, A.; Yoshida, J.; Kida, N.; Kashima, I.; Murata, W.; Enomoto, M.; Kojima, N. *Hyperfine Interact.* **2014**, *226*, 351.

(44) Sorai, M.; Nishimori, A.; Hendrickson, D. N.; Dong, T. Y.; Cohn, M. J. *J. Am. Chem. Soc.* **1987**, *109*, 4266.

(45) Surerus, K. K.; Münck, E.; Snyder, B. S.; Holm, R. H. *J. Am. Chem. Soc.* **1989**, *111*, 5501.

(46) Hush, N. S. *Prog. Inorg. Chem.* **1967**, *8*, 391.

(47) Brunschwig, B. S.; Creutz, C.; Sutin, N. *Chem. Soc. Rev.* **2002**, *31*, 168.

(48) (a) D'Alessandro, D. M.; Keene, F. R. *Chem. Soc. Rev.* **2006**, *35*, 424. (b) Nelsen, S. *Chem. - Eur. J.* **2000**, *6*, 581.

(49) (a) Demadis, K. D.; Hartshorn, C. M.; Meyer, T. J. *Chem. Rev.* **2001**, *101*, 2655. (b) Hush, N. S. *Coord. Chem. Rev.* **1985**, *64*, 135.

(50)

$$H_{AB} = \frac{2.06 \times 10^{-2} (\nu_{max}\varepsilon_{max}\Delta\nu_{1/2})^{1/2}}{r_{AB}}$$

where ν_{max} is the absorption maximum in cm^{-1}, ε_{max} is the extinction coefficient at ν_{max} in $M^{-1} cm^{-1}$, $\Delta\nu_{1/2}$ is the full width at half-maximum in cm^{-1} and r_{AB} is the electron transfer distance in Å. The value of 2.06 $\times 10^{-2} cm^{1/2} M^{1/2}$ Å is empirically determined.

(51) Ding, X.-Q.; Bominaar, E. L.; Bill, E.; Winkler, H.; Trautwein, A. X.; Drüeke, S.; Chaudhuri, P.; Wieghardt, K. *J. Chem. Phys.* **1990**, *92*, 178.

(52) Min, K. S.; DiPasquale, A. G.; Golen, J. A.; Rheingold, A. L.; Miller, J. S. *J. Am. Chem. Soc.* **2007**, *129*, 2360.

(53) Reduced magnetization data for **1** and **2** were fit using the program MagProp. See (a) Tregenna-Piggott, P. L. W. *MagProp*, version 2.0; 2008; http://www.ncnr.nist.gov/dave (part of the NIST DAVE software suite). (b) Azuah, R. T.; Kneller, L. R.; Qiu, Y. M.; Tregenna-Piggott, P. L. W.; Brown, C. M.; Copley, J. R. D.; Dimeo, R. M. *J. Res. Natl. Inst. Stand. Technol.* **2009**, *114*, 341.

(54) Here, $\hat{O}_{Fe1}$ and $\hat{O}_{Fe2}$ are the occupation operators, and T_{Fe1Fe2} is the transfer operator. See Blondin, G.; Girerd, J.-J. *Chem. Rev.* **1990**, *90*, 1359.

(55) This value was obtained from fitting variable-temperature magnetic susceptibility data with a model that neglects vibronic coupling. Upon inclusion of vibronic coupling in the model, a larger value of $B = 220 cm^{-1}$ was obtained.

(56) Kirk, M. L.; Shultz, D. A.; Schmidt, R. D.; Habel-Rodriguez, D.; Lee, H.; Lee, J. *J. Am. Chem. Soc.* **2009**, *131*, 18304.

(57) Here, we define a redox-switchable single-molecule magnet as a complex that features at least one reversible redox process and at least two isolable redox isomers, with at least one of those isomers showing slow magnetic relaxation.

(58) Freedman, D. E.; Jenkins, D. M.; Iavarone, A. T.; Long, J. R. *J. Am. Chem. Soc.* **2008**, *130*, 2884.

(59) Fortier, S.; Le Roy, J. J.; Chen, C.-H.; Vieru, V.; Murugesu, M.; Chibotaru, L. F.; Mindiola, D. J.; Caulton, K. G. *J. Am. Chem. Soc.* **2013**, *135*, 14670.

(60) (a) Liang, W.; Shores, M. P.; Bockrath, M.; Long, J. R.; Park, H. *Nature* **2002**, *417*, 725. (b) Jo, M.-H.; Grose, J. E.; Liang, W.; Baheti,

K.; Deshmukh, M. M.; Sokol, J. J.; Rumberger, E. M.; Hendrickson, D. N.; Long, J. R.; Park, H.; Ralph, D. C. *Nano Lett.* **2006**, *6*, 2014.

(61) (a) Zadrozny, J. M.; Liu, J.; Piro, N. A.; Chang, C. J.; Hill, S.; Long, J. R. *Chem. Commun.* **2012**, *48*, 3927. (b) Huang, W.; Liu, T.; Wu, D.; Cheng, J.; Ouyang, Z. W.; Duan, C. *Dalton Trans.* **2013**, *42*, 15326. (c) Colacio, E.; Ruiz, J.; Ruiz, E.; Cremades, E.; Krzystek, J.; Carretta, S.; Cano, J.; Guidi, T.; Wernsdorfer, W.; Brechin, E. K. *Angew. Chem., Int. Ed.* **2013**, *52*, 9130.

(62) (a) Freedman, D. E.; Harman, W. H.; Harris, T. D.; Long, G. J.; Chang, C. J.; Long, J. R. *J. Am. Chem. Soc.* **2010**, *132*, 1224. (b) Harman, W. H.; Harris, T. D.; Freedman, D. E.; Fong, H.; Chang, A.; Rinehart, J. D.; Ozarowski, A.; Sougrati, M. T.; Grandjean, F.; Long, G. J.; Long, J. R.; Chang, C. J. *J. Am. Chem. Soc.* **2010**, *132*, 18115.

(63) Zadrozny, J. M.; Atanasov, M.; Bryan, A. M.; Lin, C.-Y.; Rekken, B. D.; Power, P. P.; Neese, F.; Long, J. R. *Chem. Sci.* **2013**, *4*, 125.